AN EXAMINATION OF SURFACE LOCATION ERROR AND SURFACE ROUGHNESS FOR PERIOD-2 INSTABILITY IN MILLING

Andrew Honeycutt and Tony L. Schmitz
Mechanical Engineering and Engineering Science
University of North Carolina at Charlotte, Charlotte, NC

INTRODUCTION

When stable machining conditions are selected, two additional considerations for high quality part manufacture are: 1) surface location error, or part geometric errors that occur due to forced vibrations; and 2) surface roughness. Surface location error, or SLE, is the difference between the machined surface location and the commanded location. SLE is measured and/or predicted to determine the influence of (stable) machining conditions on the error. Similarly, surface roughness is an important quality metric for machined parts since it influences fatigue, sealing performance, wear, and aesthetics, for example. However, prior studies of period-n bifurcations (instabilities) have evaluated neither SLE nor surface roughness. The purpose of this paper is to predict and measure both quantities for stable and period-2 bifurcation behaviors. Time domain milling simulation is used to predict SLE and surface roughness and these results are then compared to experimental results.

PERIOD-2 MILLING BIFURCATION

Period-2 milling bifurcations represent unstable dynamic behavior with a response time period that is double the forcing time period [1-7]. In order to determine if period-2 bifurcation behavior exists, the response of the physical system is measured and then synchronously sampled at the forcing frequency. For milling, the forcing frequency is the product of the cutting tool's rotating speed and the number of teeth (i.e., the tooth passing frequency). Poincaré maps may then be used as a visual aid to interrogate the process stability.

TIME DOMAIN SIMULATION

Time domain simulation enables the numerical solution of the coupled, time-delay equations of motion for milling in small time steps [8]. It is well-suited to incorporating the inherent complexities of milling dynamics, including the nonlinearity that occurs if the tooth leaves the cut due to large amplitude vibrations and complicated tool geometries (incorporating runout, or different radii, of the cutter teeth, non-proportional teeth spacing, and variable helix). The simulation is based on the Regenerative Force, Dynamic Deflection Model described by Smith and Tlusty [9]. As opposed to analytical stability maps that provide a global picture of the stability behavior, time domain simulation provides information regarding the local cutting force and vibration behavior, including SLE [10-24] and surface roughness, for the selected cutting conditions.

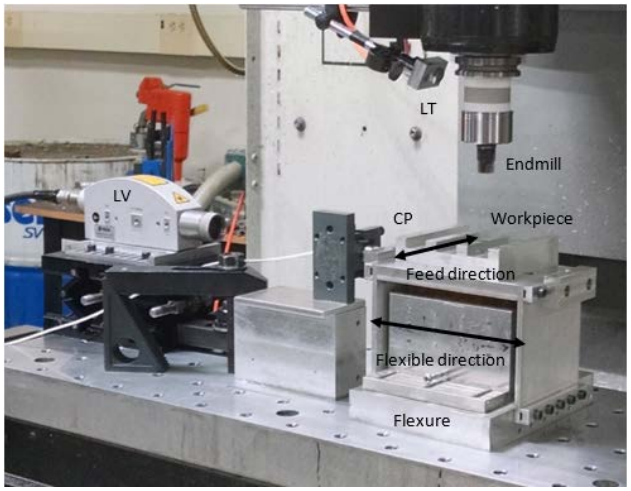

Figure 1. Flexure-based experimental setup with laser vibrometer (LV), laser tachometer (LT), and capacitance probe (CP). The feed direction and the flexible direction for the single degree of freedom flexure are also identified.

EXPERIMENTAL SETUP

The flexure-based setup displayed in Fig. 1 was used to define a physical system for simulation and testing [25-26]. The setup included a parallelogram leaf-type flexure with an aluminum workpiece mounted on top. The in-process vibration data was collected using a Polytec OFV-5000 laser vibrometer (velocity) and Lion Precision DMT20 capacitance probe (displacement). Both were aligned with the flexible direction for the single degree of freedom flexure. Note that the feed direction is perpendicular to this flexible direction. This orientation was selected to emphasize variations in surface location error and surface finish with machining conditions. Once per tooth sampling was accomplished using a laser tachometer and reflective target attached to the rotating tool holder. The flexure dynamics were

identified by modal testing: 125.8 Hz natural frequency, 0.0136 viscous damping ratio, and 1.75×10^6 N/m stiffness in the flexible (feed) direction. The dynamics for the 19.1 mm diameter, 0 deg helix angle tool (one insert) were symmetric: 1188 Hz natural frequency, 0.095 viscous damping ratio, and 4.24×10^7 N/m stiffness. The 6061-T6 aluminum alloy cutting force coefficients were: k_{tc} = 770×10^6 N/m^2, k_{nc} = 368×10^6 N/m^2, k_{te} = 22×10^3 N/m, and k_{ne} = 22×10^3 N/m. The up milling cutting conditions were: 5 mm axial depth, 2 mm radial depth, 0.35 mm/tooth, and variable spindle speed. Spindle speed values were selected to span from period-2 to stable cutting conditions while holding all other parameters constant. These spindle speeds and the corresponding behavior are listed in Table 1.

Table 1: Spindle speeds and bifurcation behavior for experiments.

Spindle speed (rpm)	Behavior	Spindle speed (rpm)	Behavior
3180	Period-2	3330	Stable
3190	Period-2	3360	Stable
3200	Period-2	3400	Stable
3210	Period-2	3500	Stable
3270	Stable	3600	Stable
3300	Stable		

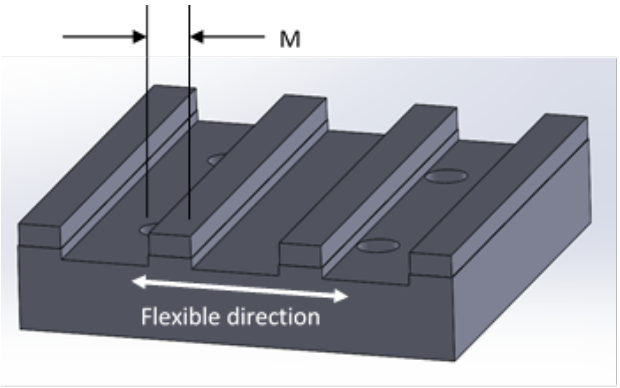

Figure 2. The workpiece included four ribs that were initially machined to the same dimensions. The {5 mm axial depth, 2 mm radial depth} cuts were then performed on one edge at a different spindle speed for each rib. The SLE was calculated as the difference between the commanded, C, and measured, M, rib widths. The flexible direction for the flexure is identified.

The workpiece geometry is presented in Fig. 2. The initial ribs were machined directly on the flexure so it could be ensured that the part was aligned with the machine axes. Low axial and radial depths were selected to minimize vibration levels and the same conditions were used to machine each rib. Prior to beginning the SLE/Ra experiments, a test workpiece was machined and the four ribs were measured on a coordinate measuring machine, or CMM, to evaluate the repeatability of the starting rib dimensions (Zeiss Prismo). The mean value was 9.82 mm with a standard deviation of 2.8 µm. Given the adequate repeatability of the initial ribs, the 11 spindle speeds in Table 1 were used to machine 11 ribs (three total workpieces). All machining conditions were identical other than spindle speed.

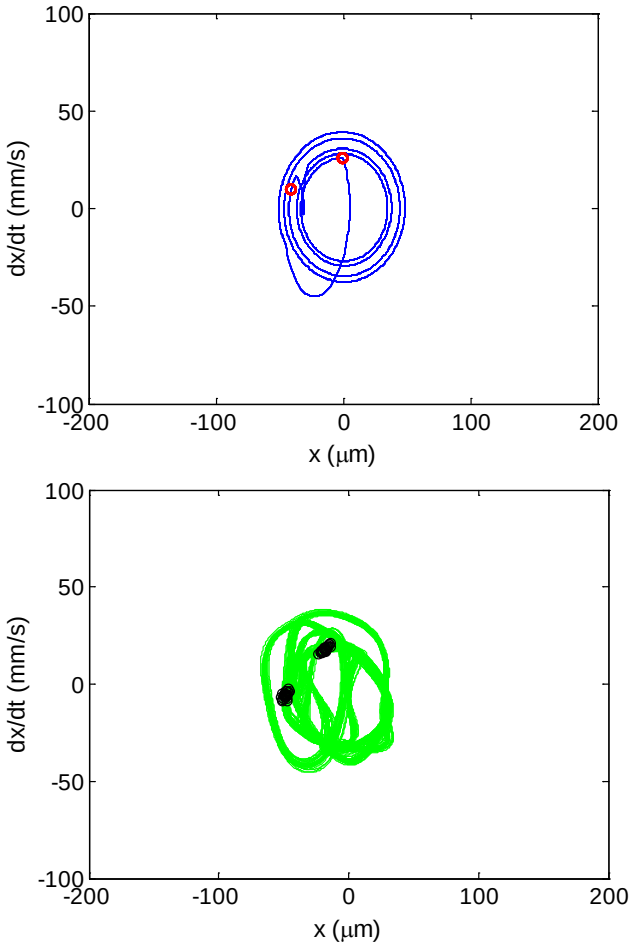

Figure 3. Predicted (Top) and measured (bottom) Poincaré maps for 3180 rpm. Period-2 behavior is seen. Note that x indicates the flexible direction for the flexure. The feed direction was y for these experiments.

The predicted and measured Poincaré maps for two of the 11 spindle speeds are presented in Figs. 3 and 4. Figure 3 displays the 3180 rpm results that exhibit

period-2 behavior. Figure 4 demonstrates stable behavior (3300 rpm).

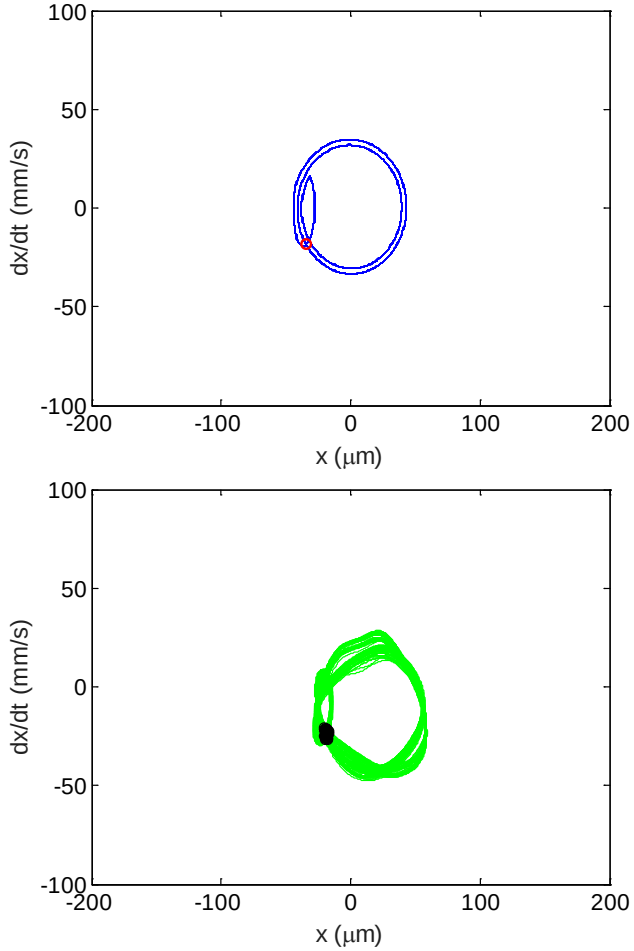

Figure 4. Predicted (left) and measured (right) Poincaré maps for 3300 rpm. Stable behavior is seen.

RESULTS

The SLE results are presented in Fig. 5. Four tests were completed under period-2 conditions (shown as the four experiment circles to the left of the dotted line) and seven were performed under stable conditions (shown as the seven experiment circles to the right of the dotted line). Good agreement is observed between the time-domain simulated prediction and the experimental behavior.

Figures 6 and 7 provide a direct comparison between the time domain simulation and the CMM surface points obtained by continuous scanning along the machined surface. In these figures the commanded surface is identified by the dashed line, the solid line is the CMM data, and the circles are the simulation results. The SLE is the difference between the commanded and actual surface and, again, good agreement is observed between simulation and measurement.

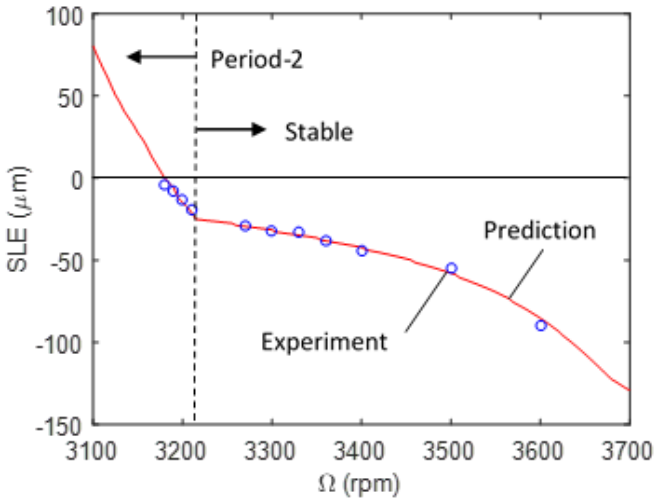

Figure 5. SLE prediction from time domain simulation (line) and experimental results from rib cutting tests (circles). The four period-2 bifurcation tests are identified.

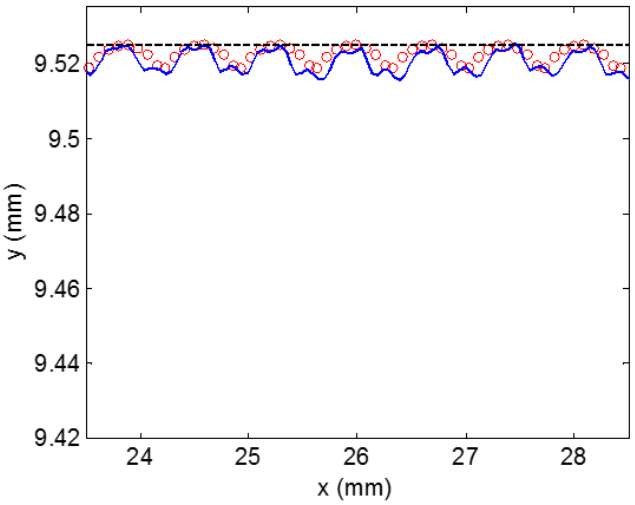

Figure 6. Commanded surface (dashed line), CMM scan (solid line), and simulation result (circles) for 3180 rpm (period-2). These results correspond to Fig. 3.

The surface roughness was also measured using a scanning white light interferometer (ZeGage, Zygo Corporation). These results are presented in Table 2, where the Ra values were calculated from a line scan at the midpoint of the axial depth of cut extracted from the surface topography. The Ra is clearly larger for

the period-2 conditions, where every other tool passage defines the surface roughness. The mean Ra for the period-2 conditions (four tests, 1.87 µm) is 5.2 times larger than the mean Ra for the stable conditions (seven tests, 0.36 µm).

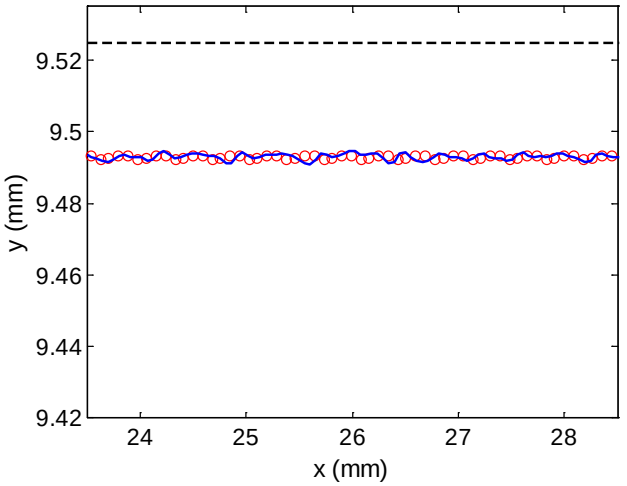

Figure 7: Commanded surface (dashed line), CMM scan (solid line), and simulation result (circles) for 3300 rpm (stable). These results correspond to Fig. 4.

Table 2. Surface roughness results for rib cutting tests.

Spindle speed (rpm)	Behavior	Ra (µm)
3180	Period-2	1.76
3190	Period-2	1.77
3200	Period-2	1.87
3210	Period-2	2.09
3270	Stable	0.28
3300	Stable	0.35
3330	Stable	0.44
3360	Stable	0.34
3400	Stable	0.39
3500	Stable	0.36
3600	Stable	0.35

The predicted and measured surface profiles are compared in Figs. 8 and 9. The change in cusp height and spacing between the period-2 (Fig. 8) and stable (Fig. 9) results is clearly seen.

The stability and SLE information is combined in Fig. 10. In this figure, the dark area represents secondary Hopf instability, the dotted area identifies the period-2 bifurcations, and the contour lines give the SLE as a function of spindle speed (horizontal axis) and axial depth of cut (vertical axis). Zero SLE is seen near the traditional best speed of 3774 rpm. However, a steep gradient for small changes in spindle speed is also seen near this speed (i.e., the zero SLE contour is vertical). A zero SLE contour is also observed within the period-2 zone. Interestingly, the SLE gradient is not as steep within the period-2 zone as it is near the best speed at 3774 rpm. This supports the possibility of producing acceptable parts under period-2 bifurcation machining conditions.

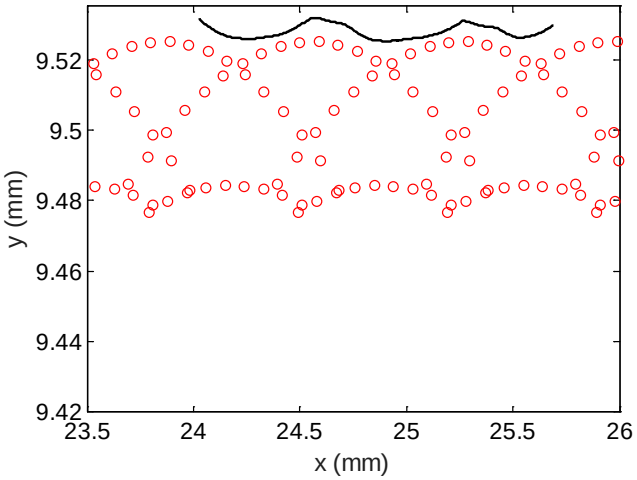

Figure 8. Scanning white light interferometer line scan (line) and simulation results (circles) for 3180 rpm (period-2).

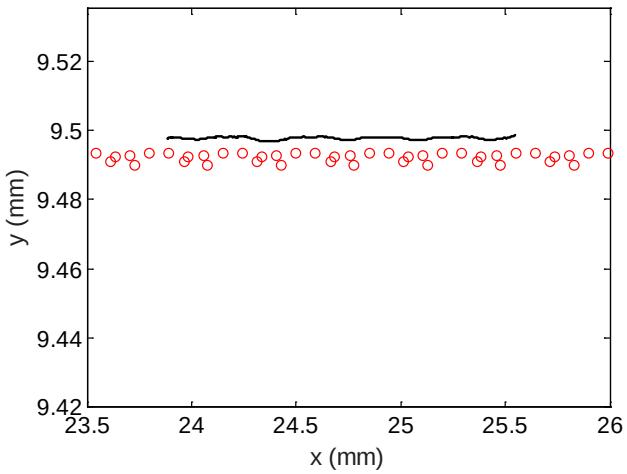

Figure 9. Scanning white light interferometer line scan (line) and simulation results (circles) for 3300 rpm (stable).

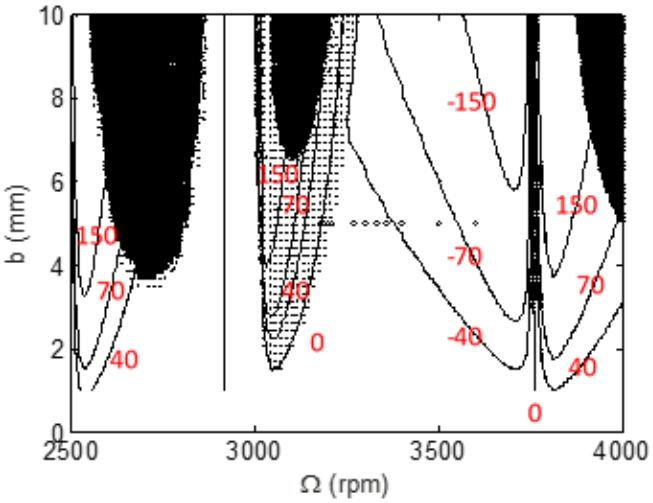

Figure 10. Combined stability and SLE map for rib cutting process dynamics. The secondary Hopf instability is represented by the dark zone, the period-2 behavior is identified by the dotted zone, and the SLE is given by the contours (i.e., lines of constant SLE).

CONCLUSIONS

Surface location error and surface roughness predictions were completed using time domain simulation for both stable and period-2 milling conditions. The predictions were compared to experiment using a flexure-based platform with displacement and velocity metrology. It was observed that the simulation accurately predicted the milling performance using: 1) Poincaré maps, which plot the displacement versus velocity and are used to identify period-2 behavior via periodic sampling; 2) surface location error measurements completed using a coordinate measuring machine; and 3) surface roughness measurements carried out using a scanning white light interferometer. It was shown that the surface location error for period-2 (unstable) behavior follows similar trends observed for (stable) forced vibration, so zero or low error conditions may be selected even for period-2 bifurcation behavior.

The surface roughness for the period-2 instability was seen to be larger than for stable conditions, although the final surface was still periodic. This increase in surface roughness occurs because the surface is defined by every other tooth passage and the apparent feed per tooth is increased.

ACKNOWLEDGEMENTS

This material is based on work supported by the National Science Foundation under Grant No. CMMI-1561221.

REFERENCES

[1] Davies, M.A., Pratt, J.R., Dutterer, B.S., and Burns, T.J., 2000, The stability of low radial immersion milling, Annals of the CIRP, 49(1): 37-40.

[2] Davies, M.A., Pratt, J.R., Dutterer, B., and Burns, T.J., 2002, Stability prediction for low radial immersion milling, Journal of Manufacturing Science and Engineering, 124: 217-225.

[3] Insperger, T. and Stépán, G., 2004, Vibration frequencies in high-speed milling processes or A positive answer to Davies, Pratt, Dutterer, and Burns, Journal of Manufacturing Science and Engineering, 126(3): 481-487.

[4] Mann, B.P., Bayly, P.V., Davies, M.A., and Halley, J.E., 2004, Limit cycles, bifurcations, and accuracy of the milling process, Journal of Sound and Vibration, 277: 31-48.

[5] Govekar, E., Gradišek, J., Kalveram, M., Insperger, T., Weinert, K., Stepan, G., and Grabec, I., 2005, On stability and dynamics of milling at small radial immersion, Annals of the CIRP, 54/1: 357-362.

[6] Honeycutt, A. and Schmitz, T., 2015, The extended milling bifurcation diagram, Procedia Manufacturing, 1: 466-476.

[7] Honeycutt, A. and Schmitz, T., 2016, A numerical and experimental investigation of period-n bifurcations in milling, Journal of Manufacturing Science and Engineering, 139(1): 011003.

[8] Schmitz, T. and Smith, K.S., 2009, Machining Dynamics: Frequency Response to Improved Productivity, Springer, New York, NY.

[9] Smith, K.S. and Tlusty, J., 1991, An overview of modeling and simulation of the milling process, Journal of Engineering for Industry, 113: 169-175.

[10] Kline, W., DeVor, R., and Shareef, I., 1982, The prediction of surface accuracy in end milling, Journal of Engineering for Industry 104: 272-278.

[11] Kline, W., DeVor, R., and Lindberg, J., 1982, The prediction of cutting forces in end milling with application to cornering cuts, International Journal of Machine Tool Design Research 22: 7-22.

[12] Tlusty, J., 1985, Effect of end milling deflections on accuracy, in: Handbook of High Speed Machining Technology (Ed. R.I. King), Chapman and Hall, New York, 140-153.

[13] Sutherland, J. and DeVor, R., 1986, An improved method for cutting force and surface error prediction in flexible end milling systems, Journal of Engineering for Industry, 108: 269-279.

[14] Montgomery, D. and Altintas, Y., 1991, Mechanism of cutting force and surface generation in dynamic milling, Journal of Engineering for Industry, 113(2): 160-168.

[15] Altintas, Y., Montgomery, D., and Budak, E., 1992, Dynamic peripheral milling of flexible structures, Journal of Engineering for Industry, 114(2): 137-145.
[16] Tarng, Y., Liao, C., and Li, H., 1994, A mechanistic model for prediction of the dynamics of cutting forces in helical end milling, International Journal of Modeling and Simulation, 14(2): 92-97.
[17] Schmitz, T. and Ziegert, J., 1999, Examination of surface location error due to phasing of cutter vibrations, Precision Engineering, 23(1): 51–62.
[18] Altintas, Y, 2000, Manufacturing Automation, Cambridge University Press, Cambridge, UK.
[19] Mann, B.P., Bayly, P.V., Davies, M.A., and Halley, J.E., 2004, Limit cycles, bifurcations, and accuracy of the milling process, Journal of Sound and Vibration, 277: 31-48.
[20] Schmitz, T., Couey, J., Marsh, E., Mauntler, N., and Hughes, D., 2007, Runout effects in milling: Surface finish, surface location error, and stability, International Journal of Machine Tools and Manufacture, 47(5): 841-851.
[21] Yun, W.-S., Ko, J., Cho, D.-W., and Ehmann, K., 2002, Development of a virtual machining system, Part 2: prediction and analysis of a machined surface error, International Journal of Machine Tools and Manufacture, 42: 1607-1615.
[22] Schmitz, T. and Mann, B., 2006, Closed-form solutions for surface location error in milling, International Journal of Machine Tools and Manufacture, 46(12-13): 1369-1377.
[23] Dombovari, Z. and Stépán, G., 2015, On the bistable zone of milling processes, Philosophical Transactions of the Royal Society A, 373: 20140409.
[24] Bachrathy, D., Munoa, J., and Stépán, G., 2016, Experimental validation of appropriate axial immersions for helical mills, The International Journal of Advanced Manufacturing Technology, 84: 1295-1302.
[25] Mann, B.P., Insperger, T., Bayly, P.V., and Stépán, G., 2003, Stability of up-milling and down-milling, Part 2: Experimental verification, International Journal of Machine Tools and Manufacture, 43(1): 35-40.
[26] Ransom, T., Honeycutt, A., and Schmitz, T., 2016, A new tunable dynamics platform for milling experiments, Precision Engineering, 44: 252-256.